Exploring beyond-mean-field logarithmic divergences in Fermi-polaron energy

R. Alhyder,[1,2,*] F. Chevy,[3,4] and X. Leyronas[3]

[1]*Center for Complex Quantum Systems, Department of Physics and Astronomy, Aarhus University, Ny Munkegade 120, DK-8000 Aarhus C, Denmark*

[2]*Institute of Science and Technology Austria (ISTA), Am Campus 1, 3400 Klosterneuburg, Austria*

[3]*Laboratoire de physique de l'Ecole Normale supérieure, ENS, Université PSL, CNRS, Sorbonne Université, Université de Paris, F-75005 Paris, France*

[4]*Institut Universitaire de France (IUF), 75005 Paris, France*

(Received 24 November 2023; accepted 28 February 2024; published 19 March 2024)

We perform a diagrammatic analysis of the energy of a mobile impurity immersed in a strongly interacting two-component Fermi gas to second order in the impurity-bath interaction. These corrections demonstrate divergent behavior in the limit of large impurity momentum. We show the fundamental processes responsible for these logarithmically divergent terms. We study the problem in the general case without any assumptions regarding the fermion-fermion interactions in the bath. We show that the divergent term can be summed up to all orders in the Fermi-Fermi interaction and that the resulting expression is equivalent to the one obtained in the few-body calculation. Finally, we provide a perturbative calculation to the second order in the Fermi-Fermi interaction, and we show the diagrams responsible for these terms.

DOI: 10.1103/PhysRevA.109.033315

I. INTRODUCTION

The physics of an impurity in a many-body ensemble is an intriguing problem, and constitutes a rich field of research in condensed matter physics. The study of the quantum impurity problem was initiated by Landau and Pekar, who proposed that the properties of conduction electrons in a dielectric medium could be understood in terms of so-called polarons, i.e., quasiparticles resulting from the dressing of the electrons by a cloud of optical phonons of the surrounding crystal [1].

More recently, the realization of spin and atomic mixtures of ultracold atoms have paved the way to the study of impurity problems in ultracold gases [2,3]. In these systems, the impurity can be immersed in either a bosonic or a fermionic medium, which leads to strikingly different behaviors and phenomena. On the one hand, since the low-lying excitation modes of a Bose-Einstein condensate (BEC) are phonons, the Bose polaron (an impurity immersed in a Bose-Einstein condensate) is quite similar to the Landau-Pekar polaron [4]. By contrast, in the Fermi-polaron case (an impurity immersed in a spin-polarized gas of fermions [5,6]) the impurity is dressed by a cloud of particle-hole pairs.

The case of an impurity immersed in a spin-1/2 superfluid was brought into the limelight following experimental works on Bose-Fermi superfluids [7–9]. As the fermion-fermion interaction is varied in the BCS-BEC crossover, the fermionic background medium evolves from a weakly attractive interaction condensate of loosely bound Cooper pairs on the BCS (Bardeen-Cooper-Schrieffer) side of the crossover to a strongly attractive interaction on the BEC side where the Fermi gas condenses in a BEC of tightly bound dimers. Thus, the polaronic state smoothly turns from a Fermi polaron on the BCS side to a Bose polaron on the BEC side of the crossover.

In the case of a zero-range coupling between the impurity and the fermions, a peculiar UV-divergent term appears when calculating the polaron energy perturbatively with respect to the impurity-fermion interaction [10,11]. This divergence is typical in three-body problems with contact interactions and was revealed first in the study of beyond-mean-field corrections in dilute Bose-Einstein condensates [12]. Indeed, three-body bound states, the Efimov trimer states, have been studied in the case of the Bose polaron [13–15]. This work is accomplished in the regime of the Born approximation with respect to the impurity-bath interaction, and therefore far from the universal regime where Efimov physics can form. However, the divergence has its origins in three-body physics and can be remedied using an effective field theory approach [16,17].

In this scheme, the divergences are suppressed by introducing counterterms corresponding to effective three-body interactions [11]. However, this renormalization process only works if the density-density response of the fermionic superfluid obeys a specific scaling that was found to be incompatible with a mean-field description of the fermionic background. This inconsistency is due to the omission of the collective mode sector in the description of the excitation spectrum of the system in the mean-field approach [11,18]. As a consequence, a proper regularization could only be carried out within the framework of random phase approximation (RPA) [18].

In this work, we compute these divergent terms rigorously in the case of an imbalanced spin-1/2 Fermi gas using Feynman diagrams from the density-density response function and we prove its behavior and relation to Tan's contact. Furthermore, we underpin the processes responsible for

*ragheed.alhyder@ist.ac.at

these divergent terms in the many-body problem without any assumptions regarding the fermion-fermion interactions in the bath. This is an important step in identifying diagrams which have signatures of the few-body physics in the problem and a step forward in understanding the polaron energy in the many-body problem.

We start by introducing the Hamiltonian of the system and a summary of the problem. Then we lay out the methodology used in identifying the dominant terms in the problem. We show that the processes responsible for the divergent behavior can be categorized in three families of diagrams for which we provide concrete arguments for their expressions in the large impurity momentum limit.

II. SYSTEM DESCRIPTION

We consider the case of an impurity immersed in a partially spin-polarized double Fermi sea at zero temperature. The imbalance between the two spin populations is chosen beyond the threshold for Clogston-Chandrasekhar transition [3,19,20], allowing us to disregard diagrams where anomalous propagators play a role. Furthermore, we assume that the impurity-fermion interaction is weak and attractive; thus, we can treat it perturbatively.

Introducing a quantization volume $\mathcal{V}$, the Hamiltonian of the system is written as

$$\begin{aligned}\hat{H} = &\sum_{\mathbf{k},\sigma} \varepsilon_k \hat{a}^\dagger_{\mathbf{k},\sigma}\hat{a}_{\mathbf{k},\sigma} + \sum_{\mathbf{q}} \varepsilon^{(i)}_q \hat{c}^\dagger_{\mathbf{q}}\hat{c}_{\mathbf{q}} \\ &+ \frac{g_0'}{\mathcal{V}} \sum_{\mathbf{k},\mathbf{q},\mathbf{k}',\mathbf{q}',\sigma} \delta_{\mathbf{k}+\mathbf{q},\mathbf{k}'+\mathbf{q}'} \hat{c}^\dagger_{\mathbf{q}'}\hat{a}^\dagger_{\mathbf{k}',\sigma}\hat{c}_{\mathbf{q}}\hat{a}_{\mathbf{k},\sigma} \\ &+ \frac{g_0}{\mathcal{V}} \sum_{\mathbf{k},\mathbf{q},\mathbf{k}',\mathbf{q}'} \delta_{\mathbf{k}+\mathbf{q},\mathbf{k}'+\mathbf{q}'} \hat{a}^\dagger_{\mathbf{k}',\uparrow}\hat{a}^\dagger_{\mathbf{q}',\downarrow}\hat{a}_{\mathbf{q},\downarrow}\hat{a}_{\mathbf{k},\uparrow}, \end{aligned} \tag{1}$$

where $\hat{a}_{\mathbf{k},\sigma}$ is the annihilation operator of a fermion with momentum $\mathbf{k}$ and spin σ, and $\hat{c}_{\mathbf{q}}$ is the annihilation operator of an impurity with momentum $\mathbf{q}$. Noting m_i and m the respective masses of the impurity and of the fermions, $\varepsilon_k = (\hbar^2 k^2)/(2m)$ is the kinetic energy of a fermion with wave vector $\mathbf{k}$ and $\varepsilon^{(i)}_q = (\hbar^2 q^2)/(2m_i)$ is the kinetic energy of the impurity with wave vector $\mathbf{q}$. g_0' and g_0 are the bare coupling constants of the fermion-impurity and the fermion-fermion interactions, respectively.

The coupling constant g_0' is related to the scattering length and the cutoff Λ through the following equation:

$$\frac{1}{g_0'} = \frac{1}{g'} - \frac{1}{\mathcal{V}} \sum_{k<\Lambda} \frac{2m_r}{\hbar^2 k^2}, \tag{2}$$

where g' is the physical coupling constant between the impurity and background fermions. It is related to the scattering length a using the relation $g' = 2\pi\hbar^2 a'/m_r$, with $m_r = (m\,m_i)/(m + m_i)$ the impurity-fermion reduced mass.

By using perturbation theory we can obtain an expression for the polaron energy up to second order [11,18]:

$$E_{\text{pol}} = g'n + \frac{g'^2 n}{\mathcal{V}} \sum_{\mathbf{q}<\Lambda} \left[\frac{2m_r}{\hbar^2 q^2} - \chi_1\left(\mathbf{q}, \epsilon^{(i)}_{\mathbf{q}}\right) \right], \tag{3}$$

where

$$\chi_1(\boldsymbol{q}, E) = \frac{1}{N} \sum_{\alpha} \frac{|\langle\alpha|\hat{n}_{\mathbf{q}}|0\rangle|^2}{(E + E_\alpha - E_0)}. \tag{4}$$

Here $\hat{n}_{\mathbf{q}} = \sum_{\mathbf{k},\sigma} a^\dagger_{\mathbf{k},\sigma} a_{\mathbf{k}+\mathbf{q},\sigma}$. $|0\rangle$ is the ground state of the interacting bath and $\{|\alpha\rangle\}$ denotes a basis of eigenvectors of the Hamiltonian of the fermionic bath alone.

It was conjectured in Ref. [11] that in the large momentum limit

$$\chi_1\left(\mathbf{q}, \varepsilon^{(\text{i})}_q\right) - \frac{1}{\varepsilon^{(\text{r})}_q} = O\left(\frac{1}{q^3}\right), \tag{5}$$

thus leading to a logarithmically divergent value of the sum appearing in Eq. (4). This divergence can be healed by introducing a three-body interaction [11] but only under the assumption that χ obeys the following asymptotic behavior:

$$\chi_1\left(\mathbf{q}, \varepsilon^{(\text{i})}_q\right) \underset{q\to\infty}{=} \frac{1}{\varepsilon^{(\text{r})}_q}\left[1 - \pi^2\kappa(\eta)\frac{m}{m_r}\frac{\mathcal{C}_2}{Nq} + \cdots\right], \tag{6}$$

where $\mathcal{C}_2$ is Tan's contact parameter of the many-body background [21], $\eta = m_{\text{i}}/m$, and

$$\begin{aligned}\kappa(\eta) &= \kappa_I(\eta) + \kappa_{II}(\eta) + \kappa_{III}(\eta) \\ &= \frac{\sqrt{\eta^3(\eta+2)}}{2\pi^3(\eta+1)^2} - \frac{\eta}{2\pi^3}\arctan\left(\frac{1}{\sqrt{\eta(\eta+2)}}\right) \\ &\quad - \frac{4}{\pi^3}\sqrt{\frac{\eta}{\eta+2}}\arctan\left(\sqrt{\frac{\eta}{\eta+2}}\right)^2. \end{aligned} \tag{7}$$

The addition of a diverging term was initially done as a conjecture with the goal of regularizing the expression in the large impurity momentum limit. This conjecture is supported by an RPA analysis of the excitation modes of the fermionic background [18] and the purpose of the present article is to prove rigorously this behavior by solving the full many-body problem and studying the processes responsible for the divergence. After a first introduction of the methodology in Sec. III, we will recover Eqs. (6) and (7) in Sec. IV using scaling arguments to generalize the results to an arbitrary order of the interaction parameter. This is supported by a perturbative analysis in the bare fermion-fermion coupling constant to identify the elementary processes by calculating exactly all diagram contributions to second order in Appendix A.

III. METHODOLOGY

The chemical potential of the impurity or equivalently the binding energy E_{pol} of the polaron is given by the self-energy of the impurity at zero momentum [22]:

$$E_{\text{pol}} = \Sigma_i(\mathbf{0}, E_{\text{pol}}). \tag{8}$$

We compute Σ_i perturbatively in $\hat{H}_{\text{int}}$ up to second order, i.e., up to order $(g_0')^2$. Note that we do not treat perturbatively the fermion-fermion interaction. The two diagrams up to order $(g_0')^2$ are shown in Figs. 1 and 2. In time and momentum representation, the impurity self-energy at first order reads

$$\Sigma^{(1)}_i(\mathbf{p}, t_2 - t_1) = \frac{g_0'}{\mathcal{V}} \sum_{\mathbf{k},\sigma} (-i) G_\sigma(\mathbf{k}, 0^-)\delta(t_2 - t_1), \tag{9}$$

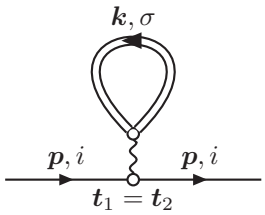

FIG. 1. The lowest-order diagram for the impurity self-energy in momentum-time representation. The open circle represents the bare impurity-fermion coupling constant g_0'. The double line represents the exact fermion Green's function G_σ. The single lines represent the impurity Green's function G_i.

where $G_\sigma(\mathbf{k}, t)$ is the exact fermion Green's function. Using $\sum_{\mathbf{k},\sigma}(-i)G_\sigma(\mathbf{k}, 0^-)/\mathcal{V} = n$, the total density we find after taking the time Fourier transform,

$$\Sigma_i^{(1)}(\mathbf{p}, E) = g_0' n. \tag{10}$$

The self-energy at second order is written in a diagrammatic form in Fig. 2; therefore, it can be written as follows:

$$\Sigma_i^{(2)}(\mathbf{p}, t_2 - t_1) = \left(\frac{g_0'}{\mathcal{V}}\right)^2 \sum_{\mathbf{q}} (-i) e^{-i\varepsilon_q^{(i)}(t_2 - t_1)} \times \langle \hat{n}_{\mathbf{p}-\mathbf{q}}(t_2)\hat{n}_{\mathbf{q}-\mathbf{p}}(t_1)\rangle \Theta(t_2 - t_1), \tag{11}$$

where we have used that the free Green's function of the impurity is $G_i^{(0)}(\mathbf{q}, t) = (-i)\Theta(t)\exp(-i\varepsilon_q^{(i)} t)$. Taking the time Fourier transform of Eq. (11), we obtain

$$\Sigma_i^{(2)}(\mathbf{p}, E) = \left(\frac{g_0'}{\mathcal{V}}\right)^2 \sum_{\mathbf{q},\alpha} \frac{|\langle\alpha|\hat{n}_{\mathbf{q}-\mathbf{p}}|0\rangle|^2}{E - \varepsilon_q^{(i)} - E_\alpha + E_0 + i\,0^+} = -\frac{{g_0'}^2 n}{\mathcal{V}} \sum_{q<\Lambda} \chi_1\left(\mathbf{q}, \epsilon_{\mathbf{q}}^{(i)}\right). \tag{12}$$

At order $(g_0')^2$, we must solve, using Eq. (8), $E_{\rm pol} = \Sigma_i^{(1)}(\mathbf{0}, E_{\rm pol}) + \Sigma_i^{(2)}(\mathbf{0}, E_{\rm pol})$. At lowest order, we can replace $E_{\rm pol}$ by 0 in $\Sigma_i^{(2)}(\mathbf{0}, E_{\rm pol})$. We express g_0' in terms of g' by expanding Eq. (2):

$$g_0' = g' + \frac{g'^2}{\mathcal{V}}\left(\sum_{\mathbf{q}}{}' \frac{2m^*}{q^2} + \cdots\right).$$

In this way, we find that $\Sigma_i^{(1)}$ gives the first term in Eq. (3), and the first term in the sum. At the same order, g_0' can be simply replaced by g' in $\Sigma_i^{(2)}$ and this term provides the contribution associated with the function χ_1 in the sum appearing in Eq. (3). Our analysis shows that with the two diagrams of Figs. 1 and 2, we recover Eq. (3).

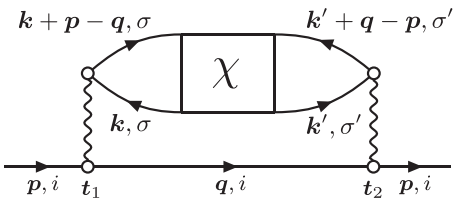

FIG. 2. The diagram for the impurity self-energy in momentum-time representation at second order in g_0'. The rectangle represents the exact density-density response function of the fermionic many-body background.

The response function χ_1 is directly related to the time-ordered density-density response function χ through

$$\chi_1\left(\mathbf{q}, \varepsilon_q^{(i)}\right) = \frac{-1}{N}\int_0^{+\infty} e^{-i\varepsilon_q^{(i)} t}\chi(-\mathbf{q}, t)dt, \tag{13}$$

where

$$\chi(\mathbf{q}, t) = -i\langle T[n_{\mathbf{q}}(t)n_{-\mathbf{q}}]\rangle. \tag{14}$$

Here, T is the time-ordering operator.

The goal is to prove the asymptotic behavior in Eq. (6), and in order to do so we will classify the Feynman diagrams contributing to the diagram in $\chi(\mathbf{q}, t)$; hence, $\lim_{|\boldsymbol{q}|\to\infty}\chi_1(\mathbf{q}, \varepsilon_q^{(i)})$.

These results hold for the case of an imbalanced Fermi gas at zero temperature. We work on expanding the diagram in Fig. 2 using the bold-diagrams formalism [23–25] in order to find the contributions that scale as $1/q^3$ in the $q \to \infty$ limit, i.e., the ones responsible for remedying the divergent term found in $\chi_1(\boldsymbol{q}, E)$.

This is achieved by taking into account the cases where (a) no interaction vertices are involved, (b) one fermionic interaction vertex is present, and (c) two fermionic interaction vertices are present in the fermionic bubble. We take inspiration for this procedure from generalizing the perturbative diagrams we have studied extensively (see Appendix A). In general, as explained in Appendix C, we do not expect any other diagrams to contribute to the diverging term. Furthermore, since no restrictions are made on the interaction nature between the fermionic particles in the bath, these results hold beyond the BCS regime.

IV. COMPUTING THE DOMINANT DIAGRAMS

In the weakly interacting limit between fermions, we study in Appendix A the perturbative diagram contributions to the divergent terms and we show the calculation for one of these contributions fully.

Here, we focus on the more general case, where no assumptions are made about the fermion-fermion interaction strength; we make qualitative arguments to distinguish the contributions to the diverging term. We can classify the diagrams contributing $\chi_1(\mathbf{q}, \varepsilon_q^{(i)})$ in three families for the diagrams of $\chi(\mathbf{q}, t > 0)$ using the bold-diagrams formalism [23–25]. The bold-diagrams formalism is a diagrammatic approach to the many-body problem where noninteracting propagators are replaced by the fully dressed Green's function G lines resulting from the resummation series, and the two-body interaction vertices are replaced by the fully dressed two-body vertices Γ. The bold diagrams are then classified in three families depending on the number of bold vertices Γ they contain. The first family contains diagrams with no bold vertices, the second family contains diagrams with one bold vertex, and the third family contains diagrams with two bold vertices. We detail the contributions of each family in the following.

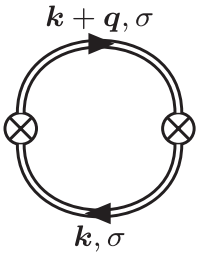

FIG. 3. The bold diagram with no vertex Γ that contributes to the density-density response function.

We define a "typical" energy scale $E_{\rm typ} = k_{\rm typ}^2/(2m)$ with the wave-vector amplitude $k_{\rm typ} = \max(|a^{-1}|, |m\mu|^{1/2})$. In the $q \gg k_{\rm typ}$ limit, we also define a cutoff ϵ in time, $\epsilon \ll 1/E_{\rm typ}$ and $q^2/m\epsilon \gg 1$, and a cutoff Λ in momentum, $\Lambda \gg k_{\rm typ}$ and $\Lambda \ll q$.

We will use the following properties of the exact Green's function $G_\sigma(\mathbf{k}, t)$ and the exact two-particle vertices $\Gamma(\mathbf{P}, t)$ of interacting fermions of the bath (see Ref. [26] for these properties in imaginary time):

Property 1. If $|p| \gg k_{\rm typ}$, $G_\sigma(\mathbf{p}, t)$ is small, except in a small interval $0 \leqslant t \lesssim (2m)/p^2$, where it tends to the Green's function of a particle in vacuum: $G_\sigma(\mathbf{p}, t) \simeq -i\Theta(t)e^{-i\frac{p^2}{2m}t}$.

Property 2. If $0 < t \ll t_{\rm typ}$, $G_\sigma(\mathbf{p}, -t) \to i n_{\mathbf{p},\sigma}$, where $n_{\mathbf{p},\sigma} = \langle c^\dagger_{\mathbf{p},\sigma} c_{\mathbf{p},\sigma}\rangle$ is the occupation number of the mode $\mathbf{p}, \sigma$.

Property 3. If $k \gg k_{\rm typ}$ and $t \lesssim m/k^2$, we can write to leading order $G_\sigma(\mathbf{k}, -t) \simeq i\frac{\mathcal{C}_2}{k^4}e^{-i\frac{k^2}{2m}t}$, where $\mathcal{C}_2$ is Tan's contact per unit volume.

Property 4. If $|\mathbf{P}| \gg k_{\rm typ}$, $\Gamma(\mathbf{P}, t)$ is small, except in a small time interval $0 \leqslant t \lesssim (4m)/P^2$, where it tends to the vertex of two particles in vacuum: $\Gamma(\mathbf{P}, t) \simeq \Gamma_{\rm vac}(\mathbf{P}, t) = -4\sqrt{\frac{\pi}{m^3 t}}e^{i\frac{\pi}{4}}e^{-i\frac{P^2}{4m}t}\Theta(t)$.

Property 5. If $0 \leqslant t \ll t_{\rm typ}$, $\int \frac{d^3P}{(2\pi)^3}\Gamma(\mathbf{P}, -t) \simeq -i\,\mathcal{C}_2/m^2$.

A. No interaction vertices

The bold diagram for $\chi(\mathbf{q}, t)$ with no two-particle vertex Γ is simply a bubble diagram with the exact Green's functions. In momentum and time variables, this diagram is given by (Fig. 3)

$$\chi_a^T(\mathbf{q}, t) = -i\sum_{\mathbf{k},\sigma} G_\sigma(\mathbf{k}+\mathbf{q}, t)G_\sigma(\mathbf{k}, -t). \tag{15}$$

From Eq. (13), we find the corresponding contribution to χ_1:

$$\chi_{1\,a}\big(\mathbf{q}, \varepsilon_q^{(i)}\big) = \sum_\sigma \frac{i}{n}\int_0^{+\infty} dt \int \frac{d^3k}{(2\pi)^3} e^{-i\varepsilon_q^{(i)}t} G_\sigma(\mathbf{k}-\mathbf{q}, t) \times G_\sigma(\mathbf{k}, -t). \tag{16}$$

$G_\sigma(\mathbf{k}, t)$ is the Green's function of a fermion with momentum $\mathbf{k}$ and spin σ. We have used $\sum_{\mathbf{k}} \to V\int d^3k/(2\pi)^3$ and $n = N/V$ the total density (V is the volume).

First, in Eq. (16) consider the contribution $t < \epsilon$ and $k < \Lambda$ in the integrals. Since $q \gg \Lambda \geqslant k$, we can replace $G_\sigma(\mathbf{k}+\mathbf{q}, t)$ by $G_\sigma(\mathbf{q}, t)$ at lowest order. If we use the first property from above, we can write $G_\sigma(\mathbf{q}, t) \simeq -i\Theta(t)e^{-i\frac{q^2}{2m}t}$ at lowest order. Since $t < \epsilon \ll t_{\rm typ}$, we can use the second property and replace at lowest order $G_\sigma(\mathbf{k}, -t)$ by $i n_{\mathbf{k}}$. Here, the integral on $\int_{|\mathbf{k}|<\Lambda}\frac{d^3k}{(2\pi)^3}n_{\mathbf{k},\sigma}$ tends to n_σ in the limit $\Lambda/k_{\rm typ} \to \infty$. We can perform the time integral on $\int_0^\epsilon dt e^{-i\frac{q^2}{2m_r}t} = (-i)(1 - e^{-i\frac{q^2}{2m_r}\epsilon})(2m_r)/q^2$. The phase $\frac{q^2}{2m_r}\epsilon \gg 1$ gives a fast oscillating term that we can neglect.

As a conclusion, the small-time, small-wave-vector contribution to Eq. (16) gives $\frac{2m_r}{q^2}$, in the $|\mathbf{q}| \to \infty$ limit.

Second, we subtract the term of order q^{-2} in Eq. (16):

$$\chi_{1\,a}\big(\mathbf{q}, \varepsilon_q^{(i)}\big) - \frac{2m_r}{q^2} = \frac{1}{n}\sum_\sigma \int_0^{+\infty} dt\, e^{-i\frac{q^2}{2m_i}t}\frac{1}{i}\int\frac{d^3k}{(2\pi)^3}\Big(G_\sigma(\mathbf{k}-\mathbf{q}, t) \times G_\sigma(\mathbf{k}, -t) - \frac{1}{i}e^{-i\frac{q^2}{2m}t}G_\sigma(\mathbf{k}, 0^-)\Big). \tag{17}$$

In the integral on the right-hand side of Eq. (17), we evaluate the contribution of the domain $\{t \in [0, \epsilon], |\mathbf{k}| > \Lambda\}$. In this domain, we can use Property 1 and replace $G_\sigma(\mathbf{k}+\mathbf{q}, t)$ with $-ie^{-i\frac{(\mathbf{k}+\mathbf{q})^2}{2m}t}$. We use Property 3 and replace $G_\sigma(\mathbf{k}, -t)$ with $i\frac{\mathcal{C}_2}{k^4}e^{-i\frac{k^2}{2m}t}$ and $G_\sigma(\mathbf{k}, 0^-)$ with $i\frac{\mathcal{C}_2}{k^4}$. We find

$$-i\int_{|\mathbf{k}|>\Lambda}\frac{d^3k}{(2\pi)^3}\frac{\mathcal{C}_2}{k^4}\int_0^\epsilon dt\left[e^{-i(\frac{q^2}{2m_i}+\frac{(\mathbf{k}+\mathbf{q})^2}{2m}+\frac{k^2}{2m})t} - e^{-i\frac{q^2}{2m_r}t}\right].$$

Neglecting fast oscillating terms, we find for the time integral $(-i)(\frac{1}{\frac{q^2}{2m_i}+\frac{(\mathbf{k}+\mathbf{q})^2}{2m}+\frac{k^2}{2m}} - \frac{2m_r}{q^2})$.

Finally, the wave-vector integral can be performed after the change of variable $\mathbf{k} \to q\mathbf{k}$. The lower bound for the norm of $\mathbf{k}$ is Λ/q, that we set to zero at lowest order. The volume element scales like q^3 and the integrand like q^{-6}. This gives the q^{-3} dependence. As a conclusion, in the $|\mathbf{q}| \to \infty$ limit, the integral on the right-hand side of Eq. (17) gives the contribution

$$-\frac{(4m\,\mathcal{C}_2\,J_a(\eta))}{n}\frac{1}{q^3},$$

where ($\hat{q}$ is a unit vector)

$$J_a(\eta) = \int\frac{d^3k}{(2\pi)^3}\frac{1}{k^4}\left(\frac{\eta}{\eta+1} - \frac{1}{\frac{1}{\eta}+(\mathbf{k}+\hat{q})^2+k^2}\right) = \frac{1}{4\pi}\frac{\sqrt{\eta^3(\eta+2)}}{(\eta+1)^2}.$$

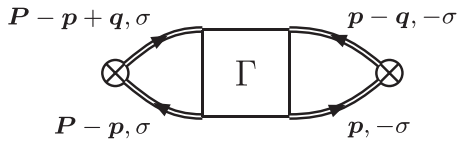

FIG. 4. The diagram with one interaction vertex and bold propagators for the fermions.

This is the dominant contribution in the $|\mathbf{q}| \to \infty$ limit as is explained below and we find

$$\chi_{1a}\left(q, \frac{q^2}{2m_i}\right) = \frac{2m_r}{q^2}\left(1 - \frac{m}{m_r}\frac{\mathcal{C}_2}{n}\frac{1}{2\pi}\frac{\sqrt{\eta^3(\eta+2)}}{(\eta+1)^2}\frac{1}{q} + \cdots\right).$$

Since $\mathcal{C}_2/n = C_2/N$, we recover in the second term the $\kappa_I(\eta)$ contribution of Eqs. (6) and (7).

B. One interaction vertex

The only diagram with one bold Γ is the diagram shown in Fig. 4. The analytic expression for $\chi_{1b}(\mathbf{q}, \varepsilon_q^{(i)})$ is

$$\chi_{1b}\left(\mathbf{q}, \varepsilon_q^{(i)}\right) = \frac{1}{n}\sum_\sigma \int_0^{+\infty} dt \int \frac{d^3p}{(2\pi)^3}\int \frac{d^3P}{(2\pi)^3}\int_{-\infty}^{+\infty} dt_1 \int_{-\infty}^{+\infty} dt_2 e^{-i\frac{q^2}{2m_i}t} G_\sigma(\mathbf{P}-\mathbf{p}-\mathbf{q}, t_1) G_\sigma(\mathbf{P}-\mathbf{p}, -t_2)$$
$$\times \Gamma(\mathbf{P}, t_2 - t_1) G_{-\sigma}(\mathbf{p}, t - t_2) G_{-\sigma}(\mathbf{p}+\mathbf{q}, t_1 - t). \tag{18}$$

In the case $|\mathbf{P}| > \Lambda$, from Property 4 we see that the dominant contribution to Γ is for $t_2 - t_1 > 0$, which contradicts the time ordering from the dominant contributions for Green's functions where $t_1 > 0$ and $t_2 < 0$. So we can neglect the contribution of the domain $|\mathbf{P}| > \Lambda$ in the integral on $\mathbf{P}$.

In the case $|\mathbf{P}| < \Lambda$, and all fermionic wave vectors larger than Λ, due to Property 1, we can replace the Green's functions by their vacuum values. In the $|\mathbf{q}| \to \infty$ limit, since the momenta are large compared to $|\mathbf{P}|$, we can set $\mathbf{P} = \mathbf{0}$ in the Green's functions. Due to the retarded nature of the fermionic Green's functions, we have the time ordering: $t_1 > 0$, $-t_2 > 0$, $t - t_2 > 0$, and $t_1 - t > 0$. For $t > 0$, the integration domain is $\{(t_1, t_2), t_1 > t, t_2 < 0\}$. Since all fermionic wave vectors are large, the dominant contributions in the time integrals come from small time differences smaller than ϵ. The time argument $t_2 - t_1$ in Γ is negative and much smaller than t_{typ}. At lowest order, we can replace $\Gamma(\mathbf{P}, t_2 - t_1)$ by $\Gamma(\mathbf{P}, 0^-)$. We define time differences $t_2' = -t_2$ and $t_1' = t_1 - t$ which vary between zero and ϵ. In the $|\mathbf{q}| \to \infty$ limit, the time t also lies between zero and ϵ, due to the $e^{-i\frac{q^2}{2m_i}t}$ in the Fourier transform of $\chi_b^T(\mathbf{q}, t)$. We have the exponential term

$$e^{-i(\frac{q^2}{2m_i} + \frac{p^2}{2m} + \frac{(\mathbf{p}+\mathbf{q})^2}{2m})t} e^{-i(\frac{(\mathbf{p}+\mathbf{q})^2}{m})t_1'} e^{-i(\frac{(\mathbf{p})^2}{m})t_2'}.$$

In Eq. (18), the integrals on time give

$$(-i)^3 \frac{1}{\frac{q^2}{2m_i} + \frac{p^2}{2m} + \frac{(\mathbf{p}+\mathbf{q})^2}{2m}} \frac{1}{\frac{(\mathbf{p}+\mathbf{q})^2}{m}} \frac{1}{\frac{(\mathbf{p})^2}{m}}.$$

Due to Property 5, the integral on $\mathbf{P}$ gives a factor $-i\mathcal{C}_2/m^2$. Finally, after rescaling of $\mathbf{p}$ by q, we also find a q^{-3} scaling and the asymptotic behavior for $\chi_{1b}(\mathbf{q}, \frac{q^2}{2m_i})$,

$$-\frac{(4m\mathcal{C}_2 J_b(\eta))}{n}\frac{1}{q^3},$$

where

$$J_b(\eta) = -\int \frac{d^3p}{(2\pi)^3}\frac{1}{\frac{1}{\eta} + p^2 + (\mathbf{p}+\hat{q})^2}\frac{1}{(\mathbf{p}+\hat{q})^2}\frac{1}{p^2}$$
$$= -\frac{1}{4\pi}\eta \arctan\left(\frac{1}{\sqrt{\eta(\eta+2)}}\right).$$

This is also the dominant contribution in the $|\mathbf{q}| \to \infty$ limit and we obtain the result

$$\chi_{1b}\left(\mathbf{q}, \frac{q^2}{2m_i}\right) = \frac{2m_r}{q^2}\frac{m}{m_r}\frac{\mathcal{C}_2}{n}\frac{1}{q}\frac{\eta}{2\pi}\arctan\left(\frac{1}{\sqrt{\eta(\eta+2)}}\right) + \cdots.$$

This is equal to the $\kappa_{II}(\eta)$ contribution in Eqs. (6) and (7).

C. Two interaction vertices

The diagrams with two bold vertices have the form in Fig. 5 with different permutations of the fermionic lines. All permutations do not contribute except for the previous diagram and the one where the two fermions connecting the interaction vertices have different spins, which has the same exact contribution resulting in a factor 2 in the final result. To this order, there exists another possible diagram for which we argue in Appendix B that it does not contribute to the divergent term. The analytic expression for this diagram is

$$\chi_c^T(\mathbf{q}, t) = -i\sum_{\sigma,\sigma'}\int_{\mathbb{R}^4}\prod_{i=1}^4 dt_i \int \frac{d^3k d^3k' d^3P}{(2\pi)^9} G_\sigma(\mathbf{k}+\mathbf{q}, t_1) G_\sigma(\mathbf{k}, -t_4) G_{-\sigma}(\mathbf{P}-\mathbf{k}, t_1 - t_4)\Gamma(\mathbf{P}+\mathbf{q}, t_2 - t_1)$$
$$\times G_{\sigma'}\left(\mathbf{k}'+\mathbf{q}, t - t_2\right) G_{\sigma'}\left(\mathbf{k}', t_3 - t\right) G_{-\sigma'}(\mathbf{P}-\mathbf{k}', t_3 - t_2)\Gamma(\mathbf{P}, t_4 - t_3) \tag{19}$$

and $\chi_{1c}(\mathbf{q}, \varepsilon_q^{(i)})$ as its time-domain Fourier transform. In the $|\mathbf{q}| \to \infty$ limit, we assume the dominant contribution to the integral comes from the high wave-vector regions. In these regions, due to Property 1 from the previous calculation, the time arguments are restricted to small positive values and the Green's functions can be replaced by vacuum values. This implies that we have the time ordering $t_1 > 0 > t_4$ and $t_3 > t > t_2$.

Next, we assume that one the two momenta of the interaction vertices is smaller than Λ. This means that we have two possibilities: either case (a), $|\mathbf{P}-\mathbf{q}| < \Lambda$ and $|\mathbf{P}| \to \infty$, or case (b), $|\mathbf{P}| < \Lambda$ and $|\mathbf{P}-\mathbf{q}| \to \infty$. In case (a), due to

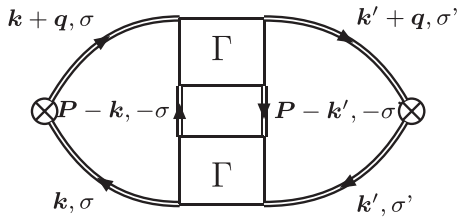

FIG. 5. The diagram with two bold interaction vertices and bold propagators for the fermions.

Property 4, we have $t_4 - t_3 > 0$. This is in contradiction with the time ordering $t_4 < 0$ and $t_3 > t > 0$, and therefore we must exclude this case.

In case (b), since $|\mathbf{P}|$ is bounded and all fermionic wave vectors tend to infinity, we can set $\mathbf{P} = \mathbf{0}$ in all of the Green's functions at lowest order. This means that $|\mathbf{P} - \mathbf{q}| \to \infty$ and we can replace $\Gamma(\mathbf{P} - \mathbf{q}, t_2 - t_1)$ by $\Gamma_{\text{vac}}(\mathbf{P} - \mathbf{q}, t_2 - t_1) \simeq \Gamma_{\text{vac}}(-\mathbf{q}, t_2 - t_1)$ due to Property 4 and the fact that $|\mathbf{P}|$ is bounded.

We define time differences which are all positive: $\tau_1 = t_1$, $\tau_2 = t_2 - t_1$, $\tau_3 = t_3 - t$, $\tau_4 = -t_4$, and $\tau_5 = t - t_2$. These time differences must be of the order of the inverse of typical kinetic energies, which are of the order $m/q^2 \ll t_{\text{typ}}$. As a consequence, we can replace the time difference $t_4 - t_3$ by 0^- in $\Gamma(\mathbf{P}, t_4 - t_3)$. The integral on $\mathbf{P}$ gives $\int_{|\mathbf{P}|<\Lambda} \frac{d^3P}{(2\pi)^3} \Gamma(\mathbf{P}, t_4 - t_3 \to 0^-) = \Gamma(\mathbf{r} = \mathbf{0}, t = 0^-) = i\frac{\mathcal{C}_2}{m^2}$, where we have used the fact that $\Lambda \gg k_{\text{typ}}$ and we extend the wave-vector integral to all space. Neglecting fast oscillating terms as before, the integral on time differences $\{\tau_i\}$ gives

$$\frac{1}{\frac{k'^2}{m}} \frac{1}{\frac{(\mathbf{k}'+\mathbf{q})^2}{2m} + \frac{(\mathbf{k}')^2}{2m} + \frac{\mathbf{q}^2}{2m_i}} \int_0^{+\infty} d\tau_2 e^{-i\frac{q^2}{2m_i}\tau_2} \Gamma_{\text{vac}}(-\mathbf{q}, \tau_2) \times \frac{1}{\frac{k^2}{m}} \frac{1}{\frac{(\mathbf{k}+\mathbf{q})^2}{2m} + \frac{(\mathbf{k})^2}{2m} + \frac{\mathbf{q}^2}{2m_i}}.$$

The upper bound on τ_2 is ϵ, but since $\epsilon q^2/(2m_i) \gg 1$, we have extended it to infinity. The integral on τ_2 can be performed analytically and is equal to $-\frac{8\pi}{m}\sqrt{\frac{\eta}{\eta+2}}\frac{1}{q} \propto \frac{1}{q}$.

The integrals on $\mathbf{k}'$ and $\mathbf{k}$ are performed after the change of variables $\mathbf{k}' \to q\mathbf{k}'$ and $\mathbf{k} \to q\mathbf{k}$. After this change of variables, we can set the lower bound Λ/q to zero at lowest order. For each integral, a factor q^3 comes from the volume element and a factor q^{-4} comes from the integrand, which makes the integral scale like q^{-1}. Together with the q^{-1} scaling of the intermediate Γ_{vac}, we recover the q^{-3} dependence.

Putting together all the factors, we find for the $|\mathbf{q}| \to \infty$ limit of the diagram in Eq. (B1) the contribution to $\chi_{1\,c}(q, \frac{q^2}{2m_i})$,

$$\frac{128\pi\, m\, \mathcal{C}_2}{n} \sqrt{\frac{\eta}{\eta+2}} (J_c(\eta))^2 \frac{1}{q^3},$$

where

$$J_c(\eta) = \int \frac{d^3k}{(2\pi)^3} \frac{1}{k^2} \frac{1}{\frac{1}{\eta} + k^2 + (\mathbf{k}+\hat{q})^2} = \frac{1}{4\pi} \arctan\sqrt{\frac{\eta}{\eta+2}}.$$

We recover the $\kappa_{III}(\eta)$ contribution in Eqs. (6) and (7).

In Appendix C, we give arguments which justify that diagrams with more than three interaction vertices give subleading contributions to $\chi_1(q, \frac{q^2}{2m_i})$ in the $q \to \infty$ limit.

V. CONCLUSION

We have calculated the leading-order contribution to the static density response function $\chi(\mathbf{q}, t)$ in the limit of large momentum transfer $|\mathbf{q}| \to \infty$ for an impurity immersed in a two-component Fermi gas with contact interaction.

We have shown that the leading-order contribution is given by the sum of three bold diagrams. The first diagram is a bubble diagram with the exact Green's functions. The second diagram contains one interaction vertex and the third diagram contains two interaction vertices. The leading-order contribution to $\chi(\mathbf{q}, t)$ in the $|\mathbf{q}| \to \infty$ limit is given by the sum of the three bold diagrams.

This helps shed light on the origin of such logarithmic divergences and provides a motivation to calculate these contributions in other cases such as the Bose polaron to see if the same behavior is present. This systematic approach has been done at zero temperature, but can also be performed at finite temperature using the same methods where similar results are expected.

ACKNOWLEDGMENTS

We thank Félix Werner and Kris Van Houcke for interesting discussions.

APPENDIX A: PERTURBATIVE LIMIT

For this approach, we will compute the response function $\chi(\mathbf{q}, \omega)$ in wave vector and frequency. We will use the formula

$$\chi_1\left(\mathbf{q}, \varepsilon_q^{(i)}\right) = \frac{i}{N} \int_{-\infty}^{+\infty} \frac{d\omega}{2\pi} \frac{\chi(-\mathbf{q}, \omega)}{\omega + \varepsilon_q^{(i)} - i\,0^+}. \tag{A1}$$

In the perturbative limit, we consider the case where the fermion-fermion interaction is weak, i.e., $g_0 \to 0^-$. In this perturbative limit, Tan's contact per unit volume is given by $\mathcal{C}_2 = m^2 g_0^2 n_\downarrow n_\uparrow$. In zeroth order, the only diagram that contributes to the polaron energy is a bubble diagram that scales as $1/q^2$ to the leading order with no q^{-3} term. To first order, the contribution of the dumbbell and tadpole diagrams in the large momentum limit are of $1/q^4$ order. This is expected since the diverging term is second order in the Fermi-Fermi interaction g_0. To second order in g_0, the diagrams that contribute to the polaron energy consist of different families which we detail in the following.

Diagrams where the two resulting fermions from the interaction with the impurity in Fig. 2 do not interact with each other. These are called the self-energy insertion diagrams since, in one of the fermionic lines, we introduce two first-order diagrams or one second-order diagram from the self-energy of the impurity. By computing all these contributions, we find that the only contributing diagram is the one in Fig. 6. In this Appendix, we show the expression for this diagram and we prove that it gives the contribution $\kappa_I(\eta)$ in Eq. (7). The diagram in Fig. 6 can be computed using the

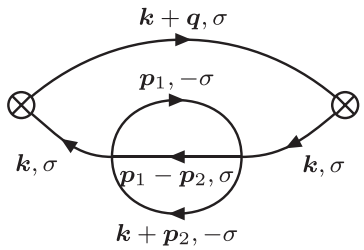

FIG. 6. A contribution to density-density response function to second order in the fermion-fermion interaction. This is the only diagram from the self-energy insertion diagrams which includes a divergent term that has a $1/q^3$ scaling.

following equation:

$$g_0^2 \sum_{k,p_1,p_2,\sigma} G_{0,\sigma}(k)^2 G_{0,-\sigma}(p_1) G_{0,\sigma}(p_1-p_2) \times G_{0,-\sigma}(k+p_2) G_{0,\sigma}(k+q). \tag{A2}$$

Remembering that all diagrams should be advanced with respect to the frequency ω we write the Green's functions product in the following manner:

$$\sum_{k,p_1,p_2} \frac{1}{(\omega_1 - E_{\boldsymbol{k}} + i\eta_1)^2} \frac{1}{\nu_1 - E_{\boldsymbol{p}_1} - i\eta} \times \frac{1}{\nu_1 - \nu_2 - E_{\boldsymbol{p}_1-\boldsymbol{p}_2} + i\eta} \frac{1}{\omega_1 + \nu_2 - E_{\boldsymbol{k}+\boldsymbol{p}_2} + i\eta} \times \frac{\theta(|\boldsymbol{k}+\boldsymbol{q}| > k_F)}{\omega_1 + \omega - E_{\boldsymbol{k}+\boldsymbol{q}} + i0^+}, \tag{A3}$$

where the sign of η and η_1 determines the boundaries for the amplitudes of the wave vectors $\boldsymbol{p}_1$, $\boldsymbol{p}_2$, and $\boldsymbol{k}$. We can first perform the integration over the frequencies ν_1 and ν_2:

$$\sum_{k,\boldsymbol{p}_1,\boldsymbol{p}_2} \frac{\theta(|\boldsymbol{k}+\boldsymbol{q}| > k_F)}{(\omega_1 - E_{\boldsymbol{k}} + i\eta_1)^2(\omega_1 + E_{\boldsymbol{p}_1} - E_{\boldsymbol{p}_1-\boldsymbol{p}_2} - E_{\boldsymbol{k}+\boldsymbol{p}_2} + i\eta)} \times \frac{1}{(\omega_1 + \omega - E_{\boldsymbol{k}+\boldsymbol{q}} + i0^+)} + \frac{1}{2\epsilon_{p_2}}. \tag{A4}$$

We found out two contributions that give the $1/q^3$ behavior:

$$\eta_1 = 0^+,\ \eta = 0^- \Rightarrow |\boldsymbol{k}| > k_F,\ |\boldsymbol{p}_1| > k_F,\ |\boldsymbol{p}_1 - \boldsymbol{p}_2| < k_F,\ |\boldsymbol{k}+\boldsymbol{p}_2| < k_F, \tag{A5}$$

$$\eta_1 = 0^-,\ \eta = 0^+ \Rightarrow |\boldsymbol{k}| < k_F,\ |\boldsymbol{p}_1| < k_F,\ |\boldsymbol{p}_1 - \boldsymbol{p}_2| > k_F,\ |\boldsymbol{k}+\boldsymbol{p}_2| > k_F. \tag{A6}$$

We make the following change of variables:

$$\boldsymbol{p}_1' = \boldsymbol{p}_1 - \boldsymbol{p}_2,\ \boldsymbol{p}_2' = \boldsymbol{k} + \boldsymbol{p}_2 \Rightarrow \boldsymbol{p}_1 = \boldsymbol{p}_1' + \boldsymbol{p}_2' - \boldsymbol{k},\ \boldsymbol{p}_2 = -\boldsymbol{k} + \boldsymbol{p}_2'.$$

First we treat the case in (A5) where $\boldsymbol{p}_1'$ and $\boldsymbol{p}_2'$ are both bounded and therefore we get the following inequalities:

$$|\boldsymbol{k}| > k_F,\ |\boldsymbol{p}_1' + \boldsymbol{p}_2' - \boldsymbol{k}| > k_F,\ |\boldsymbol{p}_1'| < k_F,\ |\boldsymbol{p}_2'| < k_F.$$

We observe from the second inequality that since $|\boldsymbol{k}|$ can go to infinity and $|\boldsymbol{p}_1'|$ and $|\boldsymbol{p}_2'|$ are bounded then the latter two are negligible for $|\boldsymbol{q}| \to \infty$, so we set $\boldsymbol{p}_1' = \boldsymbol{p}_2' = 0$ in the following and we replace $\omega = -q^2/2m_i$. We notice that the Heaviside function $\theta(|\boldsymbol{k}+\boldsymbol{q}| > k_F) = 1$ for all values of $\boldsymbol{k}$ here:

$$\sum_{k,\boldsymbol{p}_1,\boldsymbol{p}_2} \frac{1}{(\omega_1 - k^2/2m + i0^+)^2(\omega_1 + k^2/2m - i0^+)} \times \frac{1}{(\omega_1 - q^2/2m_i - (\boldsymbol{k}+\boldsymbol{q})^2/2m + i0^+)} + \frac{1}{2\epsilon_{p_2}}. \tag{A7}$$

The function has three poles with respect to ω_1 and we integrate over the upper half side of the complex plane:

$$\sum_{\boldsymbol{k},\boldsymbol{p}_1,\boldsymbol{p}_2} \frac{1}{(-q^2/2m_i - k^2/2m - (\boldsymbol{k}+\boldsymbol{q})^2/2m + i0^+)} \times \frac{1}{(-k^2/m + i0^+)^2} + \frac{1}{2\epsilon_{p_2}}. \tag{A8}$$

The two integrals over $\boldsymbol{p}_1$ and $\boldsymbol{p}_2$ give each a factor equal to the density of the Fermi gas, $n = k_F^3/6\pi^2$. Then we perform a variable change $\boldsymbol{k} = q\boldsymbol{p}$:

$$\frac{1}{q^3}\int_0^\infty \frac{d\boldsymbol{k}}{(2\pi)^3} \frac{-i}{(-k^2/m)^2(q^2/2m_i + k^2/2m + (\boldsymbol{k}+\boldsymbol{q})^2/2m)}. \tag{A9}$$

Second, we treat the case in (A6), where $\boldsymbol{p}_1'$ and $\boldsymbol{p}_2'$ are both bounded and therefore we get the following inequalities:

$$|\boldsymbol{k}| < k_F,\ |\boldsymbol{p}_1| < k_F,\ |\boldsymbol{p}_1 - \boldsymbol{p}_2| > k_F,\ |\boldsymbol{k}+\boldsymbol{p}_2| > k_F.$$

We see that $\boldsymbol{k}$ and $\boldsymbol{p}_1$ are bounded so they go to zero and we get

$$\sum_{k,\boldsymbol{p}_1,\boldsymbol{p}_2} \frac{\theta(|\boldsymbol{k}+\boldsymbol{q}| > k_F)}{(\omega_1 - E_{\boldsymbol{k}} + i\eta_1)^2(\omega_1 + E_{\boldsymbol{p}_1} - E_{\boldsymbol{p}_1-\boldsymbol{p}_2} - E_{\boldsymbol{k}+\boldsymbol{p}_2} + i\eta)} \times \frac{1}{(\omega_1 + \omega - E_{\boldsymbol{k}+\boldsymbol{q}} + i0^+)} + \frac{1}{2\epsilon_{p_2}}. \tag{A10}$$

The function has four poles with respect to ω_1 and we integrate over the upper half side of the complex plane:

$$i\frac{d}{d\omega_1} \frac{1}{(\omega_1 - q^2/2m_i + i0^+)\left(\omega_1 - p_2^2/2m_i + i0^+\right)}\bigg|_{\omega_1 = i0^+} = \frac{-i}{(q^2/2m_i)^2\left(p_2^2/m\right)} + \frac{-i}{(q^2/2m_i)\left(p_2^2/m\right)^2} \frac{1}{(-k^2/m + i0^+)^2}. \tag{A11}$$

By integrating this expression and in addition to the result of the first case we get for this diagram

$$ig_0^2\left(\frac{k_F}{6\pi^2}\right)^2 m\kappa_I(\eta)\frac{1}{q^3}$$

with $\eta = m_i/m$. This is the first contribution that appears in Eq. (6).

Other diagrams where the two interactions happen between the fermions resulting from the interaction with the impurity do not contribute except for the two diagrams shown in Figs. 7 and 8; the first one is the ladder diagram to second order while the other is the crossed ladder diagram to second order. The diagram in Fig. 7 gives the contribution in $\kappa_{II}(\eta)$. The total

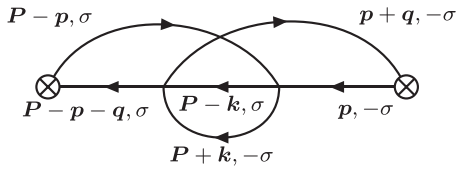

FIG. 7. Another contribution to density-density response function to second order in the fermion-fermion interaction that shows a $1/q^3$ divergent term.

momentum of the interaction vertices diverges so we have to plug in the full interaction vertex and this leads to calculating the diagram in Fig. 4, which we do in the following. Thus, the diagram has the following contribution:

$$\frac{2i}{V}\sum_{P,p}\frac{\theta(|\boldsymbol{p}|>k_F)}{\omega_1-E_{\boldsymbol{p}}+i\eta}\frac{\theta(|\boldsymbol{P}-\boldsymbol{p}-\boldsymbol{q}|>k_F)}{\Omega-\omega_1-\omega-E_{\boldsymbol{P}-\boldsymbol{p}-\boldsymbol{q}}+i\eta}\times\frac{\theta(|\boldsymbol{p}+\boldsymbol{q}|>k_F)}{\omega+\omega_1-E_{\boldsymbol{p}+\boldsymbol{q}}+i\eta}\frac{\theta(|\boldsymbol{P}-\boldsymbol{p}|>k_F)}{\Omega-\omega_1-E_{\boldsymbol{P}-\boldsymbol{p}}+i\eta}\Gamma(P), \tag{A12}$$

where $P=(\boldsymbol{P},\Omega)$, $p=(\boldsymbol{p},\omega_1)$ are internal four-momenta and $q=(\boldsymbol{q},\omega)$ is the four-momentum of the impurity.

We can write an expression for the Bethe-Salpeter equation for Γ, recalling that, at $T=0$, Feynman rules add a factor i in front of the recursive part, as follows:

$$\Gamma^{-1}(\boldsymbol{P},\Omega)=g_0^{-1}-\sum_{|\boldsymbol{p}_1|>k_F}\frac{\theta(|\boldsymbol{P}-\boldsymbol{p}_1|>k_F)}{\Omega-E_{\boldsymbol{p}_1}-E_{\boldsymbol{P}-\boldsymbol{p}_1}+i\eta}+\sum_{|\boldsymbol{p}_1|<k_F}\frac{\theta(|\boldsymbol{P}-\boldsymbol{p}_1|<k_F)}{\Omega-E_{\boldsymbol{p}_1}-E_{\boldsymbol{P}-\boldsymbol{p}_1}-i\eta} \tag{A13}$$

with $g_0^{-1}=g^{-1}-\sum_{p_1}\frac{2m^*}{p_1^2}$. We need to evaluate the expression at the frequency value $\omega=-\epsilon_{\boldsymbol{q}}$ which corresponds to the impurity's kinetic energy. Then we take the $|\boldsymbol{q}|\to\infty$ limit. For that we can write Eq. (A12) as

$$\int\frac{d^3\boldsymbol{P}}{(2\pi)^3}\int_{-\infty}^{\infty}\frac{d\Omega}{2\pi}\Gamma(\boldsymbol{P},\Omega)\,F(\Omega,\boldsymbol{P},q,k_F,m,m_i), \tag{A14}$$

where the function F is given by

$$F=\int\frac{d^3\boldsymbol{p}}{(2\pi)^3}\frac{\theta(|\boldsymbol{p}+\boldsymbol{q}|>k_F)\theta(|\boldsymbol{P}-\boldsymbol{p}|>k_F)}{(\Omega-\epsilon_{\boldsymbol{q}}-E_{\boldsymbol{P}-\boldsymbol{p}}-E_{\boldsymbol{p}+\boldsymbol{q}}+i\eta)}\times\frac{\theta(|\boldsymbol{p}|>k_F)\theta(|\boldsymbol{P}-\boldsymbol{p}-\boldsymbol{q}|>k_F)}{(\Omega-E_{\boldsymbol{P}-\boldsymbol{p}}-E_{\boldsymbol{p}}+i\eta)(\Omega-E_{\boldsymbol{p}+\boldsymbol{q}}-E_{\boldsymbol{P}-\boldsymbol{p}-\boldsymbol{q}}+i\eta)}. \tag{A15}$$

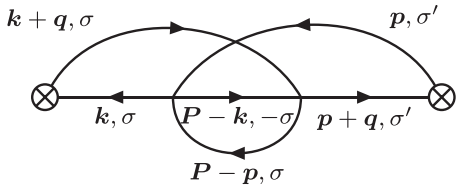

FIG. 8. Another contribution to density-density response function to second order in the fermion-fermion interaction that shows a $1/q^3$ divergent term.

We note that F is holomorphic in the upper half of the complex plane with respect to Ω. We split the complex function $\Gamma(P)$ into a sum of an advanced and a retarded function: $\Gamma(P)=\Gamma^R(P)+\Gamma^A(P)$.

The function $\Gamma^R(P)$ is holomorphic in the upper half of the complex plane and $\Gamma^A(P)$ is holomorphic in the lower half of the complex plane. With that we find that only $\Gamma^A(P)$ will contribute in Eq. (A14) in order for the integrand to not be holomorphic in the lower half plane and integrate to zero with respect to Ω. Now, we rescale $|\boldsymbol{p}|$ by $|\boldsymbol{q}|$:

$$\frac{(2m)^3}{q^3}F\left(\frac{\Omega}{q^2/(2m)},\frac{|\boldsymbol{P}|}{|\boldsymbol{q}|},1,\frac{k_F}{q},1,\frac{m}{m_i}\right).$$

By studying the behavior of the function $\Gamma(\boldsymbol{P},\Omega)$ at $|\boldsymbol{P}|,\Omega\to\infty$ we find that its limit is zero. We prove that by noticing that the second sum in Eq. (A13) is zero when $|\boldsymbol{P}|\to\infty$, we write the Heaviside function in the first sum as $1-\theta(|\boldsymbol{P}-\boldsymbol{p}_1|<k_F)$ and the second term subsequently goes to zero for $|\boldsymbol{P}|\to\infty$. We can calculate the remaining sum to find that $\Gamma^{-1}(\boldsymbol{P},\Omega)$ diverges for $|\boldsymbol{P}|,\Omega\to\infty$.

As a result, in F we can replace the first two arguments in the last expression by zero at lowest order and we find the diagram to be $\underset{|\boldsymbol{q}|\to\infty}{\propto}\frac{A}{q^3}$ with A given by

$$A=\int\frac{d^3\boldsymbol{P}}{(2\pi)^3}\int_{-\infty}^{\infty}\frac{d\Omega}{2\pi}\gamma^A_{\uparrow,\downarrow}(\boldsymbol{P},\Omega)\,(2m)^3F(0,0,1,0,m,m_i).$$

By definition we have

$$\int_{-\infty}^{\infty}\frac{d\Omega}{2\pi}\Gamma^A(\boldsymbol{P},\Omega)=\Gamma(\boldsymbol{P},t=0^-)$$

and equivalently

$$\int\frac{d^3\boldsymbol{P}}{(2\pi)^3}\Gamma(\boldsymbol{P},t=0^-)=\Gamma(\boldsymbol{r}=\boldsymbol{0},t=0^-).$$

The last expression can be related to the two-body contact as shown in Refs. [25,26] (the factor i comes from the zero-temperature formalism):

$$\mathcal{C}_2=im^2\,\Gamma(\boldsymbol{r}=\boldsymbol{0},t=0^-).$$

In this context the contact $\mathcal{C}_2$ will help us identify diverging terms as it appears as a prefactor for these terms.

With that the coefficient of the divergent term becomes

$$A=-8\,m\,\mathcal{C}_2F(0,0,1,0,m,m_i).$$

This gives one of the contributions to the divergent term in Eq. (3). With the notations used in Ref. [11] we calculate the function $F(0,0,1,0,m,m_i)$ and we find

$$F(0,0,1,0,m,m_i)=\frac{m^3}{\pi^2}\kappa_{II}(\eta),$$

where $\eta=m_i/m$ and $\kappa_{II}(\eta)=-\frac{\pi}{2}\eta\arctan(\frac{1}{\sqrt{\eta(\eta+2)}})$.

The final diagram contributes to the $\kappa_{III}(\eta)$ term. For the diagram in Fig. 8, the calculation takes the same steps but we have to pay attention that the Fermi-Fermi vertex on the right-hand side of the diagram cannot be summed perturbatively but should be replaced by the dressed vertex Γ as in the previous diagram. The relevant momentum of this vertex diverges and therefore we replace $\Gamma(P)$ by

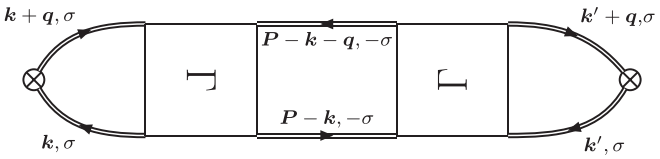

FIG. 9. The diagram with two bold interaction vertices and bold propagators for the fermions.

$-4\pi/(m\sqrt{-m(\Omega-\mathbf{P}^2/(4m)+i\,0^+)})$. We write the following expression, dominant in the $q\to\infty$ limit:

$$\sum_{P,k,p,\sigma,\sigma'} G_{0,\sigma}(k)G_{0,\sigma}(k+q)G_{0,-\sigma}(P-k)$$

$$\times G_{0,-\sigma'}(P-p)G_{0,\sigma'}(p)G_{0,\sigma'}(p+q)\Gamma(P+q)\Gamma(P)$$

$$\simeq -4\sum_{P,\boldsymbol{k},\boldsymbol{p}} \frac{4\pi\,\Gamma(P)\theta(|\boldsymbol{k}|>k_F)}{m\sqrt{-m(\Omega-q^2/2m_i-E_{\boldsymbol{k}+\boldsymbol{q}}+i0^+)}}$$

$$\times \frac{\theta(|\boldsymbol{k}+\boldsymbol{q}|>k_F)\theta(|\boldsymbol{P}-\boldsymbol{k}|>k_F)\theta(|\boldsymbol{P}-\boldsymbol{p}|>k_F)}{\Omega-E_{\boldsymbol{P}-\boldsymbol{k}}-q^2/2m_i-E_{\boldsymbol{k}+\boldsymbol{q}}+i0^+}$$

$$\times \frac{\theta(|\boldsymbol{p}|>k_F)\theta(|\boldsymbol{p}+\boldsymbol{q}|>k_F)}{\Omega-E_{\boldsymbol{P}-\boldsymbol{k}}-E_{\boldsymbol{k}}+i0^+}. \tag{A16}$$

Following the same steps as the other two calculations detailed above we get the following result:

$$\frac{128\,\pi\,m\,\mathcal{C}_2}{n}\sqrt{\frac{\eta}{\eta+2}}(J_c(\eta))^2\frac{1}{q^3}.$$

APPENDIX B: TWO INTERACTION VERTICES SUBDOMINANT DIAGRAM

A second diagram with two bold two-particle vertices Γ is shown in Fig. 9. The analytic expression is (global sign is irrelevant, since we argue that it gives a subdominant contribution in the $q\to\infty$ limit)

$$\chi_{1\,d}\big(\mathbf{q},\varepsilon_q^{(i)}\big)=\frac{\pm i}{n}\sum_{\sigma,\sigma'}\int_0^{+\infty}dt\int_{\mathbb{R}^4}\prod_{i=1}^{4}dt_i\int\frac{d^3kd^3k'd^3P}{(2\pi)^9}$$

$$\times\, e^{-i\frac{q^2}{2m_i}t}G_\sigma(\mathbf{k}-\mathbf{q},t_1)G_\sigma(\mathbf{k},-t_2)$$

$$\times\,\Gamma(\mathbf{P},t_2-t_1)G_{-\sigma}(\mathbf{P}-\mathbf{k}+\mathbf{q},t_1-t_4)$$

$$\times\, G_{-\sigma}(\mathbf{P}-\mathbf{k},t_3-t_2)\Gamma(\mathbf{P}+\mathbf{k}'-\mathbf{k},t_4-t_3)$$

$$\times\, G_\sigma(\mathbf{k}',t_3-t)G_\sigma(\mathbf{k}'-\mathbf{q},t-t_4). \tag{B1}$$

If we assume that all G's are retarded with momenta which are large, i.e., of order q, this gives seven conditions for the different times: $t_1>0$, $t_2<0$, $t_3>t_2$, $t_1>t_4$, $t>t_4$, $t_3>t$, and $t>0$. The first, sixth, and seventh conditions imply the third condition, so we have six conditions. If we assume that $|\mathbf{P}|>\Lambda$ is large, this means that the dominant contribution is for $t_2>t_1$, which is inconsistent with the conditions. Therefore, we assume $|\mathbf{P}|<\Lambda$. We find that $|\mathbf{P}+\mathbf{k}'-\mathbf{k}|\gg\Lambda$, and the dominant contribution is for $t_4>t_3$, which is inconsistent with previous conditions. As a conclusion, we find that this diagram is not dominant, compared to the diagram for $\chi_{1\,c}$.

We can recover this result in another manner. We assume that all the fermionic wave vectors of G's are of order q and are large compared to $k_{\rm typ}$. This means that at lowest order all the G's are retarded. Consider the time loop: $0\to t_1\to t_2\to 0$. Due to the retarded nature of the two G's in this loop, the time difference in Γ in this loop must be negative. This means that, at lowest order, the wave vector of the Γ in the loop cannot be large. We come to the same conclusion for the wave vector of the second Γ, by considering the time loop $t\to t_4\to t_3\to t$. Following the same procedure as before, we see that there is only one independent wave vector which is large. The integral on this large wave vector gives a factor q^3, while the integrals on the five time differences give a factor $(q^{-2})^5=q^{-10}$. This gives finally a subdominant contribution of order q^{-7}.

APPENDIX C: SUBDOMINANT DIAGRAMS WITH MORE THAN THREE VERTICES

In this section, we give arguments which justify that bold diagrams for the density-density response function with three or more two-particle vertices give a subdominant contribution in the $q\to\infty$ limit. We assume that dominant contributions in integrals come from high wave vectors (i.e., larger than $k_{\rm typ}$) of Green's functions. The Green's functions are then replaced by free particle Green's functions (indeed for negative time differences, due to Property 3, the Green's function tends to zero like the wave vector to the power -4). Consider a diagram with M two-particle vertices Γ. For $M=0$ the diagram is shown in Fig. 3; for $M=1$ it is shown in Fig. 4. The two diagrams for $M=2$ are shown in Figs. 5 and 9. The q dependence comes from three contributions. The first contribution is a "phase space" contribution: one integrates on internal wave vectors which tend to infinity and scale like q. Each three-dimensional integration gives a factor q^3. We denote N_1 the number of such independent wave vectors. The integrations give a factor q^{3N_1}. The second contribution comes from integration on "small" positive (i.e., smaller than $t_{\rm typ}$) time differences entering Green's functions. According to our hypothesis, the wave vectors are of order q and each time integration gives a factor of order q^{-2}. We denote N_2 the number of independent time differences entering Green's functions. Theses integrations give a factor q^{-2N_2}. The third contribution comes from integration on small positive time differences of Γ's, if the wave vector is "large." The time integration gives a factor q^{-1} (see Sec. IV C). We denote N_3 the number of such time differences and wave vectors. These time integrations give a factor q^{-N_3}. In total, the contribution of a diagram with numbers N_1, N_2, and N_3 scales like q^α, with

$$\alpha=3N_1-2N_2-N_3. \tag{C1}$$

As an example, for the diagram in Fig. 3, we have $M=0$, $N_1=0$, $N_2=1$, and $N_3=0$, and $\alpha=-2$. For the diagram in Fig. 4, we have $M=1$, $N_1=1$, $N_2=3$, and $N_3=0$, and $\alpha=-3$. For the diagram in Fig. 5, we have $M=2$, $N_1=2$, $N_2=4$, and $N_3=1$, and $\alpha=-3$. The diagram in Fig. 9 is subdominant. Indeed, we have seen in Appendix B that $N_1=1$, $N_2=5$, $N_3=1$, and $\alpha=-7$.

We now consider the general case, with $M \geqslant 3$ vertices Γ. There are $M+1$ independent wave vectors. N_3 wave vectors of Γ's are high and therefore there are $N_3' = M - N_3$ low wave vectors for Γ's. The total number of independent wave vectors which are high is therefore $N_1 = M + 1 - N_3' = N_3 + 1$. There are $2M+1$ independent time differences. Among these time differences, N_3 are assigned to Γ's with high momenta. We assume that all the remaining ones are assigned to G's which have high momenta and are retarded. This gives $N_2 = 2M + 1 - N_3$. We find

$$\alpha = 4N_3 - 4M + 1. \tag{C2}$$

Using this formula, we recover the results we obtained for $M = 1$ and $M = 2$. Indeed, in these cases, $N_3 = M - 1$ and $\alpha = -3$. If $N_3 \leqslant M - 2$, we find $\alpha \leqslant -7$.

For $M \geqslant 3$, we argue that $N_3 \leqslant M - 2$, or equivalently that N_3', the number of advanced Γ's, is larger than 2. Indeed, for $M = 3$, by inspection of all the possible bold diagrams, we found that at least 2 Γ's are advanced. This is due to time loops that involve one or two Γ's and Green's functions that are retarded, and we expect this will occur in general. $N_3 \leqslant M - 2$ means, using Eq. (C2), that $\alpha \leqslant -7$, and we conclude that these diagrams give subdominant contributions.

[1] L. D. Landau and S. I. Pekar, Effective mass of a polaron, Zh. Eksp. Teor. Fiz. **18**, 419 (1948).

[2] P. Massignan, M. Zaccanti, and G. M. Bruun, Polarons, dressed molecules and itinerant ferromagnetism in ultracold Fermi gases, Rep. Prog. Phys. **77**, 034401 (2014).

[3] F. Chevy and C. Mora, Ultra-cold polarized fermi gases, Rep. Prog. Phys. **73**, 112401 (2010).

[4] N. B. Jørgensen, L. Wacker, K. T. Skalmstang, M. M. Parish, J. Levinsen, R. S. Christensen, G. M. Bruun, and J. J. Arlt, Observation of attractive and repulsive polarons in a Bose-Einstein condensate, Phys. Rev. Lett. **117**, 055302 (2016).

[5] F. Chevy, Universal phase diagram of a strongly interacting Fermi gas with unbalanced spin populations, Phys. Rev. A **74**, 063628 (2006).

[6] A. Schirotzek, C.-H. Wu, A. Sommer, and M. W. Zwierlein, Observation of Fermi polarons in a tunable Fermi liquid of ultracold atoms, Phys. Rev. Lett. **102**, 230402 (2009).

[7] I. Ferrier-Barbut, M. Delehaye, S. Laurent, A. T. Grier, M. Pierce, B. S. Rem, F. Chevy, and C. Salomon, A mixture of Bose and Fermi superfluids, Science **345**, 1035 (2014).

[8] R. Roy, A. Green, R. Bowler, and S. Gupta, Two-element mixture of Bose and Fermi superfluids, Phys. Rev. Lett. **118**, 055301 (2017).

[9] X.-C. Yao, H.-Z. Chen, Y.-P. Wu, X.-P. Liu, X.-Q. Wang, X. Jiang, Y. Deng, Y.-A. Chen, and J.-W. Pan, Observation of coupled vortex lattices in a mass-imbalance Bose and Fermi superfluid mixture, Phys. Rev. Lett. **117**, 145301 (2016).

[10] W. Yi and X. Cui, Polarons in ultracold fermi superfluids, Phys. Rev. A **92**, 013620 (2015).

[11] M. Pierce, X. Leyronas, and F. Chevy, Few versus many-body physics of an impurity immersed in a superfluid of spin 1/2 attractive fermions, Phys. Rev. Lett. **123**, 080403 (2019).

[12] T. T. Wu, Ground state of a Bose system of hard spheres, Phys. Rev. **115**, 1390 (1959).

[13] J. Levinsen, M. M. Parish, and G. M. Bruun, Impurity in a Bose-Einstein condensate and the Efimov effect, Phys. Rev. Lett. **115**, 125302 (2015).

[14] M. Sun, H. Zhai, and X. Cui, Visualizing the Efimov correlation in Bose polarons, Phys. Rev. Lett. **119**, 013401 (2017).

[15] F. Grusdt, R. Schmidt, Y. E. Shchadilova, and E. Demler, Strong-coupling Bose polarons in a Bose-Einstein condensate, Phys. Rev. A **96**, 013607 (2017).

[16] E. Braaten and A. Nieto, Quantum corrections to the energy density of a homogeneous Bose gas, Eur. Phys. J. B **11**, 143 (1999).

[17] E. Braaten, H.-W. Hammer, and T. Mehen, Dilute Bose-Einstein condensate with large scattering length, Phys. Rev. Lett. **88**, 040401 (2002).

[18] A. Bigué, F. Chevy, and X. Leyronas, Mean field versus random-phase approximation calculation of the energy of an impurity immersed in a spin-1/2 superfluid, Phys. Rev. A **105**, 033314 (2022).

[19] A. M. Clogston, Upper limit for the critical field in hard superconductors, Phys. Rev. Lett. **9**, 266 (1962).

[20] B. S. Chandrasekhar, A note on the maximum critical field of high-field superconductors, Appl. Phys. Lett. **1**, 7 (1962).

[21] S. Tan, Large momentum part of a strongly correlated Fermi gas, Ann. Phys. **323**, 2971 (2008).

[22] R. Combescot, A. Recati, C. Lobo, and F. Chevy, Normal state of highly polarized Fermi gases: Simple many-body approaches, Phys. Rev. Lett. **98**, 180402 (2007).

[23] N. V. Prokof'ev and B. V. Svistunov, Bold diagrammatic Monte Carlo: A generic sign-problem tolerant technique for polaron models and possibly interacting many-body problems, Phys. Rev. B **77**, 125101 (2008).

[24] K. Van Houcke, F. Werner, E. Kozik, N. Prokof'ev, B. Svistunov, M. J. H. Ku, A. T. Sommer, L. W. Cheuk, A. Schirotzek, and M. W. Zwierlein, Feynman diagrams versus Fermi-gas Feynman emulator, Nat. Phys. **8**, 366 (2012).

[25] R. Rossi, T. Ohgoe, E. Kozik, N. Prokof'ev, B. Svistunov, K. Van Houcke, and F. Werner, Contact and momentum distribution of the unitary Fermi gas, Phys. Rev. Lett. **121**, 130406 (2018).

[26] K. Van Houcke, F. Werner, T. Ohgoe, N. V. Prokof'ev, and B. V. Svistunov, Diagrammatic Monte Carlo algorithm for the resonant Fermi gas, Phys. Rev. B **99**, 035140 (2019).